UV Resonance Raman Determination of Protein Acid Denaturation: Selective Unfolding of Helical Segments of Horse Myoglobin†

Zhenhuan Chi and Sanford A. Asher*

Department of Chemistry, University of Pittsburgh, Pittsburgh, Pennsylvania 15260

Received May 16, 1997; Revised Manuscript Received October 29, 1997

ABSTRACT: We have used UV resonance Raman spectroscopy to study the acid denaturation of horse heart aquometmyoglobin (Mb) between pH 7.5 and 1.5. Raman spectra excited at 206.5 nm are dominated by amide vibrations, which are analyzed by using a new methodology to quantitatively determine the Mb secondary structure. In contrast, the 229-nm Raman spectra are dominated by the Tyr and Trp Raman bands, which are analyzed to examine changes in Tyr and Trp environments, such as exposure to water, hydrogen bonding, and, for Trp, any alterations of the dihedral angle between the Trp ring and its linkage to the protein backbone. We uniquely determined which Mb α-helices melt by combining the amide, Tyr, and Trp Raman spectral information with heme absorption spectral information. We calculate that the Mb α-helical composition decreases from ∼80% at neutral pH to ∼19% below pH 3.5. The Trp Raman cross sections dramatically decrease at low pH to values which indicate that they are fully exposed to water; this result indicates that the A helix melts. The Tyr Raman bands are pH independent, which indicates that the G and H helices around the Tyr residues do not melt. The dramatic heme absorption acid denaturation changes indicate major alterations of the heme pocket and changes in heme binding. These results indicate that the A, B, C, D, E, and F helices melt in a concerted fashion, while the antiparallel G and H helices only partially melt.

The understanding of protein structure and dynamics is challenged by the present lack of insight into the mechanism(s) by which proteins self-assemble from their primary sequences of linked amino acids to form three-dimensional functional enzymes with well-defined secondary, tertiary, and quaternary protein structures (*1*−*8*). Numerous studies of protein folding and unfolding have utilized a host of techniques, including NMR, CD, absorption, and fluorescence spectroscopy (*2, 9*−*18*). These studies, which attempted to elucidate the rules for protein folding (and unfolding), utilized highly sensitive and selective techniques to examine static and dynamic aspects of protein structural changes.

In this report, we apply UV resonance Raman spectroscopy to determine the Mb secondary structural changes during acid denaturation. The work here utilizes a new amide resonance Raman spectroscopic methodology (*19, 20*), which quantitatively determines protein secondary structure, to examine the intermediate unfolded state of horse heart aquometmyoglobin (Mb). Mb has often been used as a paradigm for protein folding and unfolding because Mb shows a well-defined intermediate unfolded form which still retains some α-helical structure (*11, 13, 21*−*24*). In addition, Mb investigations greatly benefit from the immense amounts of structural information which already exist for this protein.

We have examined the acid-induced denaturation of Mb by monitoring the UV Raman spectra of both the amide vibrations and the Tyr and Trp aromatic amino acid vibrations, as well as the heme Soret band absorption spectra. We utilize the new pure secondary structure Raman spectral methodology, described in the preceding paper in this issue, to determine the pH dependence of the Mb secondary structure. We use the Tyr and Trp bands observed in the 229-nm excited UV Raman spectra (*20, 26*−*32*) as markers to determine whether the helices to which they are attached melt. Changes in particular Trp and/or Tyr environments, such as solvent exposure and hydrogen bonding, correlate with secondary structural changes at the Trp and Tyr attachment sites. We compare this information with the heme absorption results to conclude that the A, B, C, D, E, and F helices melt, while the G and H helices remain mostly intact, especially around the Tyr residues.

Our results on holoMb, which indicate that all but the G and H helices melt, differ from conclusions of previous studies, using other techniques (*11, 13*), on the acid denaturation of sperm whale apoMb; these studies suggested that the A, G, and H helices remain intact. The differences between horse holoMb and sperm whale apoMb may result from stronger interactions between the A helix and the G and H helices in the apoMb since the heme pocket collapses and permits more intimate interactions between the A, G, and H helices. Alternatively, a fundamental stability difference may exist between horse and sperm whale Mb, since Gruebele recently observed melting of the A helix in horse apoMb (*33*).

* To whom correspondence should be addressed. Phone: (412) 624-8570. Fax: (412) 624-0588. E-mail: asher+@pitt.edu.

† We gratefully acknowledge financial support from the National Institute of Health through Grant No. R01GM30741-15.

S0006-2960(97)01161-6 CCC: $15.00
Published on Web 02/12/1998

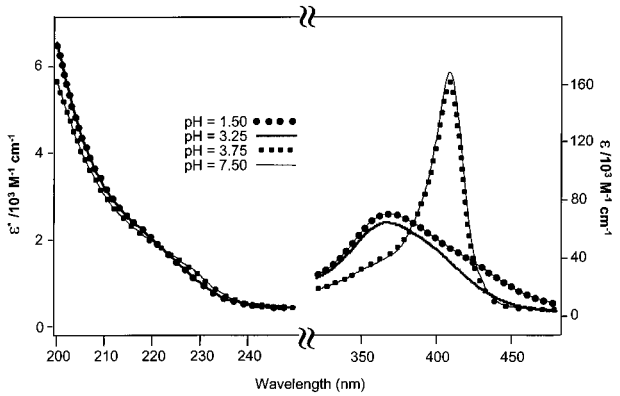

FIGURE 1: Aquometmyoglobin (30 μM) absorption spectra at various pH values. The spectra were measured in a 0.5-mm-path length cell. ϵ* is the molar absorptivity in unit of peptide bond concentration.

EXPERIMENTAL SECTION

Horse heart metmyoglobin (Mb), *N*-acetyl-tyrosine ethyl ester (Ac-Tyr-ee), and *N*-acetyl-tryptophan ethyl ester (Ac-Trp-ee) were purchased from Sigma Chemical Co. (St. Louis, MO) and used as received. We utilized 18 μM Mb solutions for Raman spectra excited at 206.5 nm and 91 μM Mb solutions for 229-nm excitation. The sample solution pH value was adjusted by adding small amounts of concentrated HCl and KOH solutions with rapid stirring. We used the ~500-cm^{-1} water librational band (*34*) as an internal intensity standard to determine absolute Raman cross sections because we found that the Mb aggregated in acid solutions below pH 2.5 in the presence of 0.15 M perchlorate. We separately determined the water librational Raman band cross section by measuring the relative intensity of this band compared to that of perchlorate. The 2249-cm^{-1} acetonitrile band previously determined by Dudik et al. (*35*) was used to calculate the Raman cross sections of Ac-Trp-ee and Ac-Tyr-ee in the water/propanol solvent.

UV Raman measurements were obtained by using instrumentation described in detail previously (*36, 37*). CW laser excitation at 206.5 (2.5 mW) and 229 nm (9 mW) were obtained from intracavity frequency-doubled Kr ion and Ar ion lasers, respectively (*36, 38*). For the higher concentration (1.5 mg/mL) 229-nm excitation experiments, we used a wire-guided jet sampling system similar to that of Cho et al. to avoid photoaggregation (*39*). For the lower concentration 206.5-nm excitation experiments, the sample solutions were pumped through a 1.0-mm-i.d. Supersil quartz capillary. A 1800 grooves/mm grating was used in second order. Spectral resolutions were 8.5 cm^{-1} for 229-nm excitation and 20 cm^{-1} for 206.5-nm excitation, respectively. Absorption spectra were measured by using a Perkin-Elmer Lamda-9 spectrometer.

RESULTS

Acidification of Mb solutions below pH 4 has long been known to cause unfolding (*11, 13, 16, 17, 20*−*24*). This unfolding causes large changes in the heme crevice, as shown by the Figure 1 pH dependence of the aquometMb absorption spectra. The neutral pH aquometMb absorption spectrum shows a strong heme Soret band at 409 nm, while Tyr and Trp absorption bands occur between 260 and 300 nm (not shown), and the stronger Tyr and Trp absorption bands appear as a shoulder between 210 and 230 nm (*39*−*41*). The region below 220 nm is dominated by the $\pi\rightarrow\pi$* absorption of the protein amide backbone linkages (*18, 42, 43*).

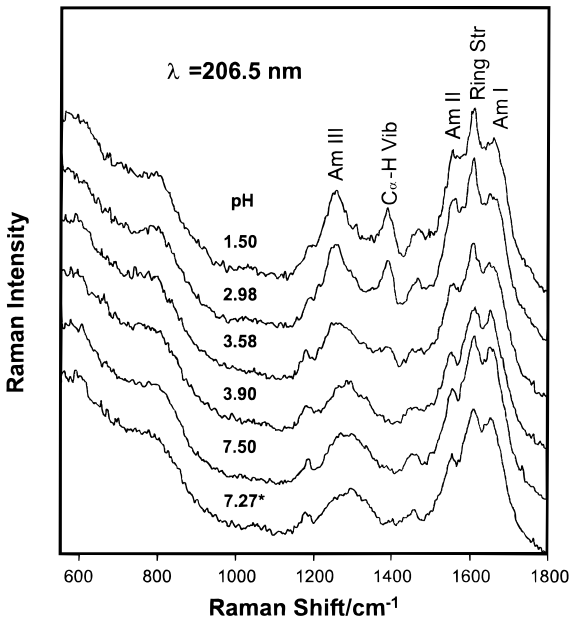

FIGURE 2: 206.5-nm excited Raman spectra of aquometmyoglobin (18 μM) at various pH values. The pH 7.27 sample was cycled to acid pH and then returned to pH 7.27. Power is 2.5 mW. The spectra were detected by an ICCD detector, with a total accumulation time of 20 min. A 1800 grooves/mm grating was used in second order, giving a spectral resolution of ~20 cm^{-1}.

The absorption spectra are independent of pH between pH 7.5 and ~3.5. However, a pH decrease to below 3.5 results in an increased absorption between 200 and 220 nm and a decreased absorption around 230 nm. These spectral changes correlate with the known unfolding of the dominantly Mb α-helical structure (81%) (*44*); the absorption increase below 220 nm results from hyperchromism of the amide $\pi\rightarrow\pi$* electronic transitions due to decreased excitonic interactions in the unfolded unordered conformation(s) compared to those in the α-helix conformation (*18, 43*).

The small ca. 230-nm Mb absorption decrease results from acid denaturation alterations in the environments of the Tyr and Trp residues which shift their aromatic ring $\pi\rightarrow\pi$* transition frequencies (vide infra). The neutral pH 409-nm Soret band absorbance decreases and is replaced with a more diffuse 363-nm Soret band; these results indicate major changes in heme binding.

Figure 2 shows the 206.5-nm excited resonance Raman spectra of Mb at pH values between 7.50 and 1.50. The 206.5-nm excited Raman spectra are dominated by the amide vibrations (*18, 36*), since this excitation is resonant with the amide $\pi\rightarrow\pi$* transitions. The spectra show strong enhancement of the amide I vibration (~1660 cm^{-1}), which is predominantly carbonyl stretching; enhancement of the ring stretching vibrations of the Tyr and Trp aromatic amino acid side chains (~1610 cm^{-1}) (*19, 25*−*31*); strong enhancement of the amide II vibration (1555 cm^{-1}), which involves all the atoms of the amide group but contains a large contribu-

tion of C−N stretching and N−H bending; a variable intensity of the amide C_α−H bending vibration (1386 cm^{-1}); and strong enhancement of the amide III vibration (1240−1300 cm^{-1}), whose composition is similar to that of the amide II vibration, except that opposite phasing occurs between C−N stretching and N−H bending (*43*, *45*, *46*).

The Mb amide Raman spectra are essentially identical between pH 7.50 and 3.90; the spectra show a strong amide I (1655 cm^{-1}) band and medium-intensity amide II (1555 cm^{-1}) and III (1290 cm^{-1}) bands. No band near 1386 cm^{-1} is evident, due to the fact that the Mb secondary structure is mainly α-helical (*18*, *36*, *43*). The invariance of the Raman frequencies, intensities, and band shapes indicates little change in the protein secondary structure between pH 7.50 and 3.90.

Below pH 3.9, the 1386-cm^{-1} amide C_α−H bending band appears, which indicates a significant unraveling of the Mb α-helical structure. The amide III band frequency shifts from 1290 to 1268 cm^{-1} between pH 3.9 and 3.58, and it further shifts to 1261 cm^{-1} at pH 2.98. The amide III band Raman cross section increases from 26 mbarn $molecule^{-1}$ sr^{-1} at pH 3.98 to 39 mbarn $molecule^{-1}$ sr^{-1} at pH 2.98. The amide I band shifts 7 cm^{-1} to lower frequency, and its Raman cross section slightly decreases. The amide II band frequency remains relatively constant, while its Raman cross section increases from 27 to 46 mbarn/$molecule^{-1}$ sr^{-1} . A further pH decrease to 1.50 causes little additional Raman spectral changes, which indicates little further change of the Mb secondary structure.

The bottom Figure 2 Mb spectrum, which is of a sample where the pH was first adjusted from neutrality down to pH 1.50 and then adjusted back to pH 7.27, is identical with that at pH 7.50. This clearly indicates that the acid-induced unfolding is reversible over the time frame of our measurement (20 min).

In the previous accompanying paper, we demonstrated a new methodology to determine protein secondary structure, which utilizes a set of calculated 206.5-nm UV Raman spectra (PSSRS) of the pure α-helix, β-sheet, and unordered secondary structures (*19*). These PSSRS are used to model the measured protein Raman spectra to quantitatively determine the protein secondary structure composition. This is a robust determination since we simultaneously utilize the amide I, II, and III bands and the C_α−H amide bending bands to determine secondary structure (*18*).

We utilized this methodology here to determine the Mb secondary structure composition at the different pH values. Prior to modeling, we subtract from the observed protein spectrum both the Raman spectrum of water and the Tyr, Trp, and Phe aromatic side-chain ring Raman bands, as previously described (*18*). In addition, we do not include the ∼1610 and the ∼1450-cm^{-1} spectral regions in the modeling calculation. Figure 3 shows the measured Mb spectra used for the modeling as well as the residuals between the measured and calculated spectra.

The small values of the residuals demonstrate that these three PSSRS fit all the Mb spectra very well and that even the low-pH acid-denatured Mb unfolded state is mainly composed of these three secondary structures. However, the lowest pH spectra show clear residual features, such as the broad peak at ∼1250 cm^{-1} and the broad trough at 1680 cm^{-1}, which indicate formation of additional secondary structural motifs which are not well modeled by the three existing PSSRS.

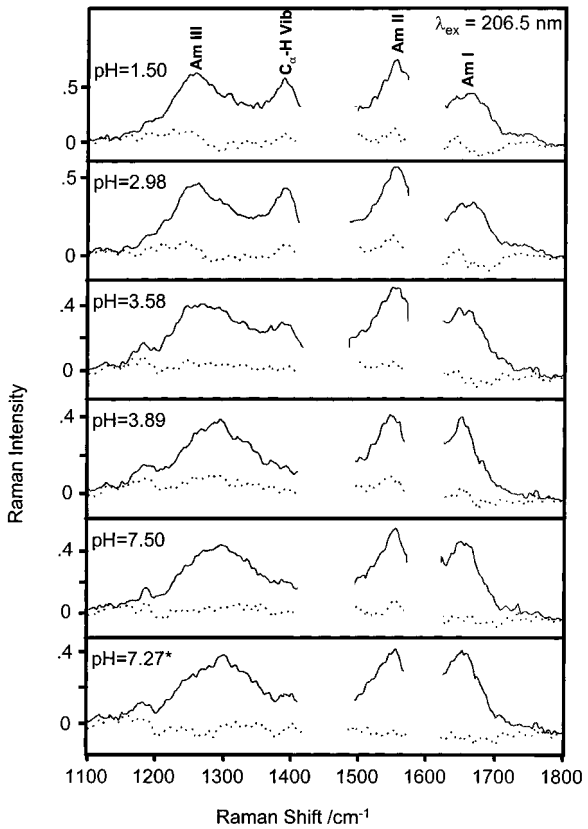

FIGURE 3: Spectral modeling of the measured 206.5-nm excited Raman spectra (—) of aquometmyoglobin (18 μM) at various pH values and the residuals (···) (1100−1800 cm^{-1}). Prior to modeling, we subtract from the observed protein spectrum both the Raman spectra of water and the Tyr, Trp, and Phe side chains, as previous described (*18*). In addition, we neglect the ∼1610- and the ∼1450-cm^{-1} spectral regions.

Table 1: Horse Myoglobin Secondary Structure Composition at Various pHs

pH	α-helix (%)	β-sheet (%)	unordered
1.50	19	0	81
2.98	19	0	81
3.58	44	9	46
3.90	78	0	22
4.52	77	0	23
5.05	73	0	27
7.50	73	0	27
7.27r	78	0	22

Table 1, which lists our calculated Mb secondary structure fractional abundances at the different pH values, indicates that Mb switches from predominantly α-helical to unordered structures during the acid denaturation process. The only exception is the pH 3.58 sample, which is calculated to have 9% β-sheet structure. This sample shows small residual features over the entire 1200−1400-cm^{-1} spectral region. This may indicate the occurrence of unusual secondary structure(s) at this pH, which is at the midpoint of the cooperative unfolding transition. Figure 4, which displays the pH dependence of Mb α-helical composition, indicates a relatively constant ∼75% calculated α-helix composition from pH 7.50 to 3.90, which drops to 19% α-helix at pH 3. We put constraints on fitting of pH <3 Mb spectra, since unconstrained fits of the unfolded (pH < 3) Mb spectra give

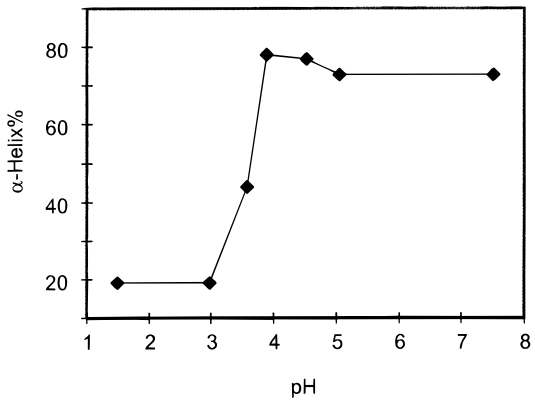

FIGURE 4: pH dependence of the calculated Mb α-helical composition.

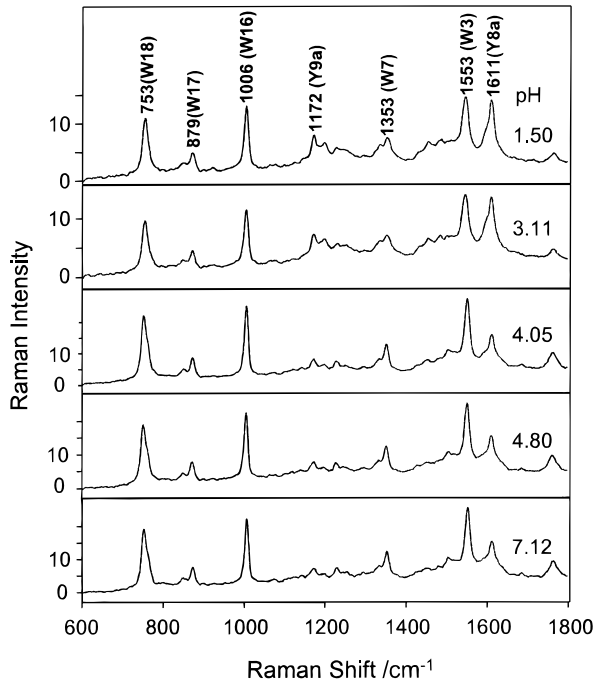

FIGURE 5: 229-nm excited Raman spectra of horse aquometmyoglobin (91 μM) at various pH values. Power, 9 mW. The spectra were detected by an ICCD detector, with a total accumulation time of 10 min. A 1800 grooves/mm grating was used in second order, giving a spectral resolution of ~8.5 cm^{-1}.

rise to negative helical composition value, because our fitting modeling does not include all of the structural motifs in the unfolded Mb spectra.

Additional information on the pH-induced conformational changes can be obtained by studying the change in the Raman spectra of the aromatic amino acid bands. Although contributions of Tyr, Trp, and Phe occur at ~1610 cm^{-1} in the 206.5-nm excited Raman spectra, this spectral region is strongly overlapped by the amide bands.

Excitation at 229 nm within the strong Tyr and Trp $\pi \rightarrow \pi^*$ transitions results in selective enhancement of Tyr and Trp bands (*25*−*31*, *41*), with negligible interference from either the amide bands or any bands from other amino acid side chains. Figure 5 shows the 229-nm excited Raman spectra of Mb at various pH values. The 759-, 857-, 879-, 1012-, 1339-, 1359-, 1453-, 1516-, and 1557-cm^{-1} bands derive from Trp, while the 1179-, and 1207-cm^{-1} bands derive from Tyr. The 1613-cm^{-1} band derives mainly from the Tyr Y8a band, but a small contribution also occurs from the Trp W1 band (*39*).

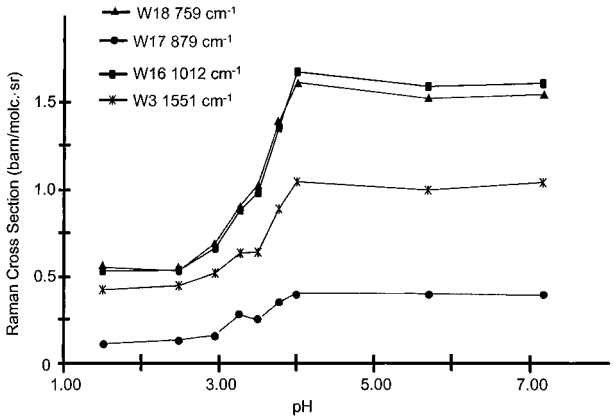

FIGURE 6: pH dependence of 229-nm excited Mb Trp Raman cross sections. The water band at 500 cm^{-1} was used as an internal intensity standard to determine the Raman cross sections. 229-nm excited Raman cross sections of *N*-acetyl-tryptophan ethyl ester in aqueous solution: W18 (759 cm^{-1}), 0.574; W17 (879 cm^{-1}), 0.130; W16 (1012 cm^{-1}), 0.509; W3 (1551 cm^{-1}), 0.383 (10^{-24} cm^2 $molecule^{-1}$ sr^{-1}), respectively.

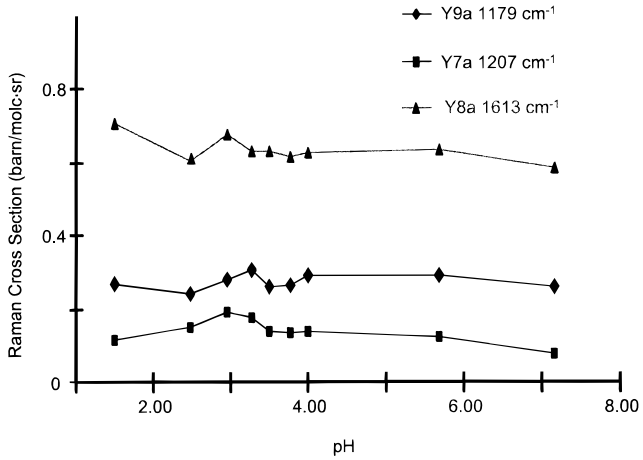

FIGURE 7: pH dependence of 229-nm excited Mb Tyr Raman cross sections. The water band at 500 cm^{-1} was used as an internal intensity standard to determine Raman cross section. 229-nm excited Raman cross sections of *N*-acetyl-tyrosine ethyl ester in aqueous solution: Y9a (1179 cm^{-1}) 0.16; Y7a (1207 cm^{-1}), 0.053; Y8a (1613 cm^{-1}), 0.38 (10^{-24} cm^2 $molecule^{-1}$ sr^{-1}), respectively.

The intensities of the Trp but not the Tyr bands decrease as the pH decreases, as indicated by Figures 6 and 7, which plot the pH dependence of the Trp and Tyr Raman cross sections. The cross sections of the 759-, 879-, 1012-, and 1551-cm^{-1} Trp bands decrease by almost 3-fold as the pH decreases below 4.0. This decrease levels off by pH 2.50.

To interpret these data, we investigated the environmental dependence of the Tyr and Trp Raman and absorption spectra. Figures 8 and 9 show the UV absorption spectrum of Trp and Tyr in water, methanol, and *n*-propanol. The strong $\pi-\pi^*$ transition of Trp at ~220 nm derives from a transition to the B_b state. Tyr has a strong $\pi-\pi^*$ transition band at ~190 nm, which derives from transitions to the B_a and B_b states, and a strong $\pi-\pi^*$ transition band at ~220 nm, which derives from the transition to the L_a state.

The Trp and Tyr absorption bands red-shift as the solvent changes from water to methanol and to propanol. These spectral redshifts are similar to those observed by Cho et al.

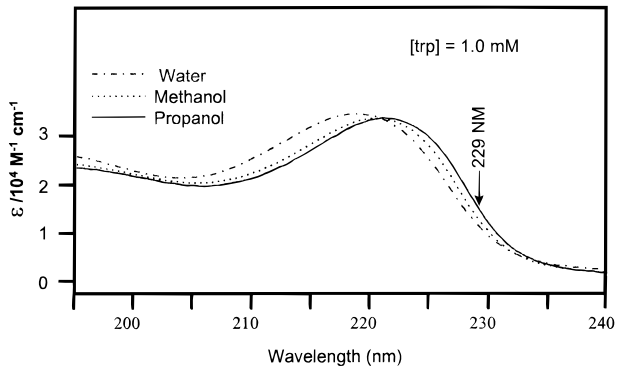

FIGURE 8: UV absorption spectra of 1.0 mM *N*-acetyl-tryptophan ethyl ester in water, methanol, and propanol solution. Path length, 0.5 mm.

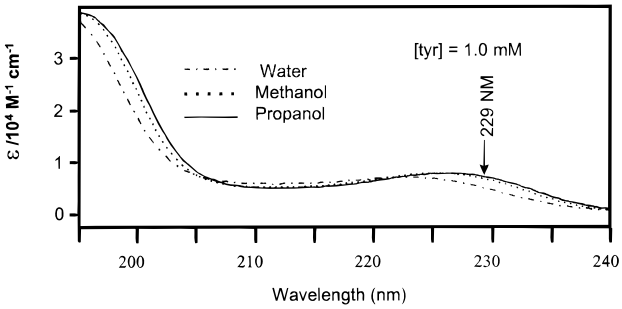

FIGURE 9: UV absorption spectra of 1.0 mM *N*-acetyl-tyrosine ethyl ester in water, methanol, and propanol solution. Path length, 0.5 mm.

(*39*), which they showed were related to an increased magnitude of the solvent H-bond accepting ability or the solvent H-bond-donating ability. Whatever the case, polar solvents tend to stabilize the ground states of Trp and Tyr more than less polar solvents and thus give rise to shorter wavelength $\pi-\pi^*$ transitions. Since we excite the Trp and Tyr spectra on the red edge of their Raman excitation profile maxima, we expect a decrease in their Raman cross sections if the Tyr and Trp residues exchange from a buried to a water-exposed environment; the Raman excitation profile maximum will blue-shift away from the 229-nm excitation wavelength. The decrease of Trp Raman cross section in Mb during acid denaturation to a value almost identical with that of Trp in water indicates that the Trp becomes exposed to water upon Mb unfolding (*47*). The Mb Tyr residues Raman cross sections remain ~2-fold larger than those of blocked Tyr in water.

To confirm the dependence of Trp and Tyr band Raman cross sections on solvent exposure, we measured the dependence of the Ac-Trp-ee and Ac-Tyr-ee Raman cross sections upon solvent composition. We measured the 229-nm excited Raman spectra of Ac-Trp-ee and Ac-Tyr-ee in a water/propanol binary solvent. Raman spectra of water/propanol solvent mixtures which contain 5% acetonitrile as an intensity standard were used to determine the Raman cross sections of the Trp and Tyr bands. Figure 10 shows the solvent dependence of the 229-nm excited Ac-Trp-ee band (W3, W16, and W18) Raman cross sections of in water/propanol solvent, while Figure 11 shows the solvent dependence of 229-nm excited Ac-Tyr-ee band (Y7a, Y8a, and Y9a) Raman cross sections in water/propanol solvent. These two figures demonstrate that the Raman cross sections of the Trp and Tyr band decrease as the water composition

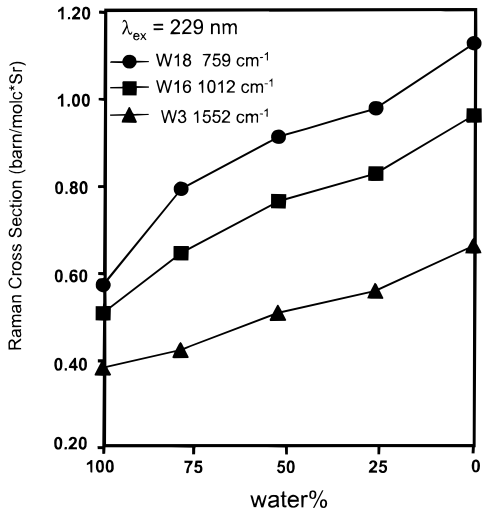

FIGURE 10: Solvent dependence of the 229-nm excited Raman cross sections of *N*-acetyl tryptophan ethyl ester in water/propanol solvent.

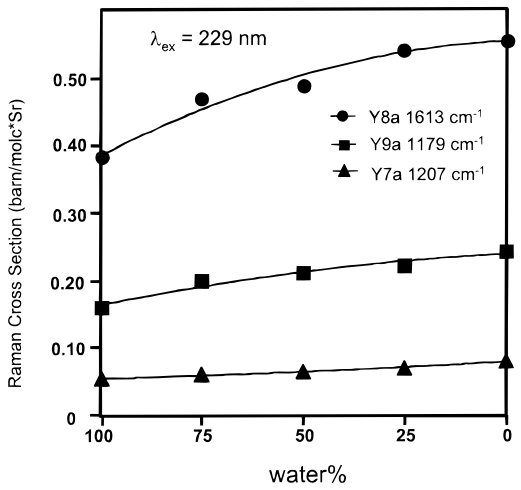

FIGURE 11: Solvent dependence of the 229-nm excited Raman cross sections of *N*-acetyl tyrosine ethyl ester in water/propanol solvent.

increases. Thus, the Raman cross sections of Trp and Tyr in proteins will decrease as they become exposed to water when the protein unfolds.

A band shape change is evident for the ~1557-cm^{-1} Trp W3 Raman band (*48*) upon acid denaturation. At neutral pH, this band is asymmetric, with a bandwidth of 15.7 cm^{-1}. At acid pH, the frequency decreases to 1553 cm^{-1}, and the band becomes more symmetric, with a bandwidth of 19.7 cm^{-1}. The W3 band frequency is known to depend on the angle $\chi^{2,1}$, which links the C_γ in the indole ring to the C_β of the amino acid side chain (*48*).

The observed Trp Raman band results from overlapping contributions from the two Mb Trp within the A helix. We can deconvolute this neutral pH Trp W3 band into two bands at 1553.6 and 1558.6 cm^{-1}, with relative intensities of about 1:2. This leads to $\chi^{2,1}$ angles of ~102° and >120°, respectively, which can be compared to X-ray diffraction results for Trp7 and Trp14 of 100° and 150°, respectively (*44*). We thus assign the 1553.6- and 1558.6-cm^{-1} bands to Trp7 and Trp14, respectively. This assignment is also consistent with the relative Raman cross sections found in the deconvoluted spectrum; the Raman cross section of the Trp7 band is ~60% that of Trp14. The surface-accessible

FIGURE 12: Ribbon diagram of horse heart myoglobin. The eight helices are label by letters A−H. The heme group and the trp7, trp14, tyr103, tyr146, distal His64, and proximal His93 are shown (*44*).

areas are calculated to be 56 and 22 Å^2 for trp7 and trp14, respectively (*44*, *49*). The more water exposed Trp should have a blue-shifted excitation profile and a lower Raman cross section. The slightly broader but symmetric W3 Trp band at acidic pH is consistent with almost identical $\chi^{2,1}$ angles for the two Trp of ~110°, but with apparently larger distributions in angles.

The Raman cross section changes and the W3 frequency and band shape clearly signal that the environments of both Trp are dramatically altered upon Mb unfolding (vide infra). The lack of Tyr Raman cross section, frequency, or band shape changes upon acid unfolding indicates that the microenvironments of the Tyr residues do not change during the acid denaturation. Since the two Tyr are located on the Mb G and H helixes, these results indicate no melting of the G and H helixes around the Tyr residues.

DISCUSSION

Horse heart Mb is a globular, single-domain protein of 153 amino acids (Figure 12), which possesses eight rodlike α-helical segments of varied length (labeled as A−H). Horse heart Mb contains two Trp (trp7 and trp14 in helix A) and two Tyr residues (tyr103 and tyr146 in helices G and H, respectively). The B, C, E, and F helices frame the heme pocket (*44*).

The Tyr and Trp side chains in the native protein are predominantly buried, with little contact with water. Some of the flanking side chains, like Lys, have larger hydrogen-bond-acceptor abilities. Native Mb shows water solvent surface-accessible areas of 56, 22, 38 and 2 Å^2 for the Trp7, Trp14, Tyr103, and Tyr146 residues, respectively (*44*, *49*), while the Trp and Tyr rings in the glycine-blocked Trp and Tyr tripeptide show surface-accessible areas of 217 and 187 Å^2, respectively (*51*). Thus, in native aquometMb, 74% of trp7 and 90% of trp14 are buried, while 80% of tyr103 and 99% of tyr146 are buried.

Figures 6 and 7 show that the 229-nm Raman cross sections of Trp and Tyr bands in native Mb are approximately 3 and 2 times larger than those of blocked Trp and Tyr in aqueous solution, respectively. The fact that the Raman cross sections of Trp in Mb at pH 1.5 are essentially identical with that of blocked Trp in aqueous solution suggests that the Trp in the unfolded protein are essentially fully exposed to water.

In the absence of tertiary contacts, helix A would have calculated solvent surface-accessible areas for trp7 and trp14 of 122 and 132 Å^2, which is about half that of Gly-Trp-Gly (217 Å^2). Thus, approximately half of these rings are buried by the adjacent A helix amino acid side chains and half by the tertiary contacts with other side chains.

The Raman intensity alterations observed require that the native Mb tertiary and secondary structures that are responsible for burying the Trp disappear upon acid denaturation. Thus, we conclude that helix A, which contains the two Trp (trp7 and trp14), totally melts at acidic pH.

The lack of Tyr Raman band changes indicates that helices G and H remain folded in highly acidic conditions and preserve their tertiary contacts, especially around the Tyr residues. The Gly-Tyr-Gly side-chain solvent surface-accessible area of 187 Å^2 is decreased to 38 and 2 Å^2 for tyr103 and tyr146 in native Mb, respectively. The contacts within the G and H helices and the tertiary contacts between them bury areas of 90 and 150 Å^2. The remaining tertiary contacts are responsible for burying the remaining 59 and 35 Å^2. Thus, essentially all of the Tyr protecting tertiary contacts in native Mb are preserved in the acid unfolded protein.

While we have not, as yet, thoroughly quantified the dependence of the Raman cross section of Tyr and Trp on aqueous exposure, we have demonstrated in Figures 10 and 11 that the Raman cross sections of Trp and Tyr depend on water exposure and that the Raman cross section dependence results from the Raman excitation profile shifts, which result directly from the absorption spectral shifts. In addition, we know that these shifts are probably most related to environmental hydrogen-bonding acceptance values (*39*, *51*). Our observed absorption spectral shifts appear to be approximately proportional to changes in solvent composition. Thus, we can assume $\sigma = \sigma_w + F\Delta\sigma_p$, where σ_w is the Raman cross section of the residue in water, $\Delta\sigma_p$ is the increase in Raman cross section for fully burying the residue, and F is the fractional solvent exposure. We can detect a 5% change in Raman cross section; thus, we suggest that less than ~10 Å^2 of the Tyr surface area becomes exposed to water.

The dramatic changes in the Soret band in Mb, shown in Figure 1, indicates dramatic structural changes in the B, C, D, E, and F helices framing the heme pocket. As the pH decreases, the 409-nm Soret band absorption disappears and a new broad 363-nm band appears; the proximal His93 on helix F protonates and the iron changes from five- to six-coordinate, where water molecules weakly bind to both sides. This behavior is consistent with the unraveling of the B, C, D, E, and F helices, which has been suggested previously (*20*, *23*, *24*).

The residual 19% α-helical structure composition observed at low pH is significantly less than that which would be contributed by the native G and H helices alone (29% α-helical structure). Thus, we conclude that parts of the G and H helices localized away from the Tyr residues also melt, and that the A, B, C, D, E, and F helices entirely melt. Our results indicate that the acid denaturation of Mb involves a cooperative simultaneous melting of most of the α-helical segments of Mb at pH ~3.5, with the exception of ~66%

of the G and H helices, the portions localized around the Tyr residues.

The unique stability of the G and H helices and their connecting hairpin loop is likely to be due to interactions between their hydrophobic faces, which contain Ile101, Leu104, Phe138, Ile142, and Tyr146 near the C-terminal end and Ile111, Ile112 ,and Leu135 approximately in the middle of the helices. This is consistent with the observation that the G−H helical fragment of Mb and unfolded residues form partially stable α-helix structures in aqueous solution and extensive α-helical structures in the presence of the helix promoter trifluoroethanol (*51*, *52*). Furthermore, the G−H helices should also be stabilized by the antiparallel alignment of the macrodipole moments of the G and H helices.

Previous studies of sperm whale apomyoglobin (ApoMb) indicated that the A, G, and H helices remain α-helical following acid denaturation (*11*, *13*), which differs from our results, where we conclude that helix A melts. This difference could result from the structural difference between holoMb and ApoMb. Since the heme group is absent in apoMb, stronger interactions between the A helix and helices G and H may occur to stabilize helix A at low pH in apoMb. In the holoprotein, the constraints of accommodating the heme group may prevent significant interactions between helix A and helices G and H in Mb. However, our preliminary studies of the acid denaturation of horse apoMb also indicate the unfolding of the A helix (*47*). Alternatively, the difference may result from the primary sequence difference between sperm whale and horse Mb. We find it comforting that Gruebele have recently concluded that the horse apoMb A helix melts upon cold denaturation (*33*). We will report on the acid denaturation of horse apoMb and sperm whale holo- and apoMb in the future.

CONCLUSIONS

We have demonstrated a methodology to monitor the secondary structure unfolding of specific helical segments of Mb by modeling the UV Raman spectra of the protein backbone amide bands. In addition, we probe the Tyr and Trp UV Raman spectra to obtain insight on environmental changes for these aromatic amino acids which may signal localized amide backbone conformation changes. We conclude that, for holoMb, acid-induced denaturation involves unfolding of helices A−F at pH ∼3.5, while the helices G and H still retain some α-helical structure, especially around the Tyr residues. We presume that this melting of the helices framing the heme pocket is responsible for the observed change in heme binding. The sensitivity of the Trp and Tyr 229-nm Raman cross sections to their environment mainly results from the dependence of Raman excitation profile peak maxima (due to the dependence of the absorption λ_{max}) on the aromatic amino acid environments. We demonstrate here that the Raman cross sections of the Trp and Tyr residues can be used as markers for their local exposure to water. This technique can be extended to probe secondary structural changes at chosen locales within a protein by using site-directed mutagenesis to attach Tyr or Trp marker residues.

ACKNOWLEDGMENT

We are pleased to acknowledge helpful conversations with Prof. Martin Gruebele and Dr. Pusheng Li.

REFERENCES

1. Dill, K. A., and Chan, H. S. (1997) *Nature Struct. Biol. 4*, 10.
2. Gilmanshin, R., Williams, S., Callender, R. H., Woodruff, W. H., and Dyer, B. (1997) *Proc. Natl. Acad. Sci. U.S.A. 94*, 3709.
3. Fischer, D., Rice, D., Bowte, J. U., and Eisenberg, D. (1995*) FASEB J. 10*, 126.
4. Thornton, J. M., Jones, D. T., MacArthur, M. W., Orengo, C. M., and Swindells, M. B. (1995) *Phil. Trans. R. Soc. London B 348*, 71.
5. Creighton, T. E. (1992) *Protein Folding*, W. H. Freeman and Co., New York.
6. Creighton, T. E. (1993) *Proteins: Structures and Molecular Properties*, W. H. Freeman and Co., New York.
7. Kyte, J. (1995) *Structure in Protein Chemistry*, Garland Publishing: New York.
8. Kim, P. S., and Baldwin, R. L. (1990) *Annu. Rev. Biochem. 59*, 631.
9. Ballew, R., Sabelko, J., and Gruebele, M. (1996) *Proc. Natl. Acad. Sci. U.S.A. 93*, 5759.
10. Venyaminov, S. Y., and Yang, J. T. (1995) in *Circular Dichroism and the Conformational Analysis of Biomolecules* (Fasman, G. D., Ed.), pp 69, Plenum Press, New York and London.
11. Jennings, P. A., and Wright, P. E. (1993) *Science 262*, 892.
12. Eftink, M. R. (1991) *Methods Biochem. Anal. 35*, 127.
13. Hughson, F. M., Wright, P. E., and Baldwin, R. L. (1990) *Science 249*, 1544.
14. Johnson, W. C., Jr. (1996) in *Circular Dichroism and the Conformational Analysis of Biomolecules* (Fasman, G. D. Ed.) pp 635−654, Plenum Press, New York and London.
15. Roder, H. and Wuthrich, K. (1986) *Proteins*: *Struct., Funct., Genet. 34*, 563.
16. Acampora, G., Hermans, J., Jr. (1967) *J. Am. Chem. Soc. 89*, 1543.
17. Roder, H., Elove, G. A., and Englander, W. (1988) *Nature 335*, 700.
18. Acampora, G., and Hermans, J., Jr. (1967) *J. Am. Chem. Soc. 89*, 1550.
19. Chi, Z., Chen, X. G., Holtz, J. S. W., and Asher, S. A. (1998) *Biochemistry 37*, 2854−2864.
20. Asher, S. A., Johnson, C. R., and Murtaugh, J. (1983) *Rev. Sci. Instrum. 54*, 1657.
21. Palaniappan, V., and Bocian, D. F. (1994) *Biochemistry 33*, 14264.
22. Barrick, D., and Baldwin, R. L. (1993) *Biochemistry 32*, 3790.
23. Barrick, D., and Baldwin, R. L. (1993) *Protein Sci. 2*, 869.
24. Sage, J. T., Morikis, D., and Champion, P. M. (1991) *Biochemistry 30*, 1227.
25. Han, S., Rousseau, D. L., Giacometti, G., Brunori, M. (1990) *Proc. Natl. Acad. Sci. U.S.A. 87*, 205.
26. Sweeney, J. A., and Asher, S. A. (1990) *J. Phys. Chem. 94*, 4784.
27. Ludwig, M., and Asher, S. A. (1988) *J. Am. Chem. Soc. 110*, 1005.
28. Larkin, P. J., Gustafson, W. G., Asher, S. A. (1991) *J. Chem. Phys. 94*, 5324.
29. Johnson, C. R., Ludwig, M. L., and Asher, S. A. (1986) *J. Am. Chem. Soc. 108*, 905.
30. Asher S. A., Larkin, P. J., and Teraoka, J. (1991) *Biochemistry 30*, 5944.
31. Rava, R. P., and Spiro, T. G. (1985) *J. Phys. Chem. 89*, 1856.
32. Rava, R. P., and Spiro, T. G. (1984) *J. Am. Chem. Soc. 106*, 4062.
33. Gruebele, M. (1997), personal communication.
34. Walrafen, G. E. (1972) in *Water, A Comprehensive Treatise* Vol. 1, Chapter 5, (Franks, F., Ed.) Plenum Press, New York.
35. Dudik, J. M., Johnson, C. R., and Asher, S. A. (1985) *J. Chem. Phys. 82*, 1732.
36. Holtz, J. S. W., Bormett, R. W., Chi, Z., Cho, N., Chen, X. G., Pajini, V., Asher, S. A., Arrogoni, M., Owen, P., and Spinelli, L. (1996) *Appl. Spectrosc. 50*, 1459.
37. Asher, S. A., Ludwig, M. L., and Johnson, C. R. (1986) *J. Am. Chem. Soc. 108*, 3186.

38. Asher, S. A., Bormett, R. W., Chen, X. G., Lemmon, D. H., Cho, N., Peterson, P., Arrigoni, M., Spinelli M., and Cannon, J. (1993) *Appl. Spectrosc. 47*, 628.
39. Cho, N, Song, S., and Asher, S. A. (1994) *Biochemistry 33*, 5932.
40. Asher, S. A., and Chi, Z. (1997) in *Biomolecular Structure and Dynamics* (Vergoten, G., Ed.) pp 263, NATO ASI Series, Kluwer Academic Publishers, Boston.
41. Cho, N., and Asher, S. A. (1996) *Biospectroscopy 2*, 71.
42. Rosenheck, K., and Doty, P. (1961) *Proc. Natl. Acad. Sci. U.S.A. 47*, 1775.
43. Song, S., and Asher, S. A. (1989) *J. Am. Chem. Soc. 111*, 4295.
44. Evans, S. V., and Brayer, G. D. (1988) *J. Biol. Chem. 263*, 4263.
45. Chen, X. G., Asher, S. A., Scheitzer-Stenner, R., Mirkin, N. G., and Krimm, S. (1995) *J. Am. Chem. Soc. 117*, 2884.
46. Chen, X. G., Scheitzer-Stenner, R., Asher, S. A., Mirkin, N. G., and Krimm, S. (1995) *J. Phys. Chem. 99*, 3074.
47. Chi, Z., and Asher, S. A. (1998) *J. Am. Chem. Soc.* (submitted).
48. Miura, T., Takeuchi, H., and Harada, I. (1989) *J. Raman Spectrosc. 20*, 667.
49. Lee, B., and Richards, F. M. (1971) *J. Mol. Biol. 55*, 379.
50. Miller, S., Janin, J., Lesk, A. M., and Chothia, C. (1987) *J. Mol. Biol. 196*, 644.
51. Kamlet, M. J., Abboud, G. L. M., and Taft, R. W. (1981) *Prog. Phys. Org. Chem. 13*, 485.
52. Shin, H.-C., Merutka, G., Waltho, J. P., Tennant, L. L., Dyson, H. J., and Wright, P. E. (1993) *Biochemistry 32*, 6356.
53. Soennichsen, F. D., VanEyk, J. E., Hodges, R. S., and Sykes, B. D. (1992) *Biochemistry 31*, 8791.

BI971161R